AD-A126 007 EVALUATION OF THE TROPICAL CYCLONE SPIRAL LINEARIZATION TECHNIQUE(U) NAVAL ENVIRONMENTAL PREDICTION RESEARCH FACILITY MONTEREY CA S D SWADLEY FEB 83 NEPRF-TR-83-04 1/1

UNCLASSIFIED F/G 4/2 NL

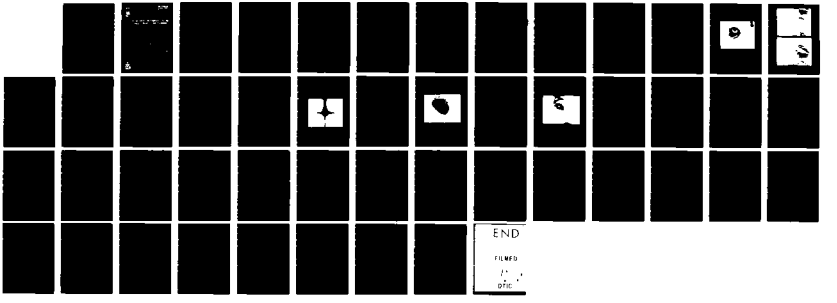

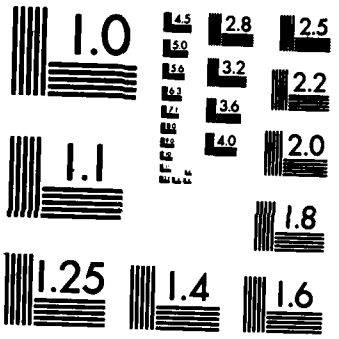

EVALUATION OF THE TROPICAL CYCLONE SPIRAL LINEARIZATION TECHNIQUE

Steven D. Swadley
Naval Environmental Prediction Research Facility

FEBRUARY 1983

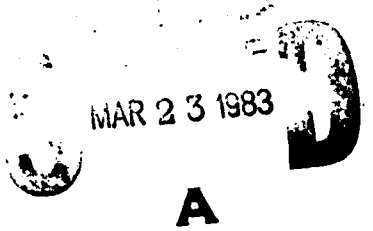

NAVAL ENVIRONMENTAL PREDICTION RESEARCH FACILITY
MONTEREY, CALIFORNIA 93940

UNCLASSIFIED

SECURITY CLASSIFICATION OF THIS PAGE (When Data Entered)

REPORT DOCUMENTATION PAGE		READ INSTRUCTIONS BEFORE COMPLETING FORM
1. REPORT NUMBER NAVENVPREDRSCHFAC Technical Report TR 83-04	2. GOVT ACCESSION NO. AD-A126007	3. RECIPIENT'S CATALOG NUMBER
4. TITLE (and Subtitle) Evaluation of the Tropical Cyclone Spiral Linearization Technique		5. TYPE OF REPORT & PERIOD COVERED Final
		6. PERFORMING ORG. REPORT NUMBER TR 83-04
7. AUTHOR(s) Steven D. Swadley		8. CONTRACT OR GRANT NUMBER(s)
9. PERFORMING ORGANIZATION NAME AND ADDRESS Naval Environmental Prediction Research Facility Monterey, CA 93940		10. PROGRAM ELEMENT, PROJECT, TASK AREA & WORK UNIT NUMBERS PE 62759N PN WF59-553 NEPRF WU 6.2-16
11. CONTROLLING OFFICE NAME AND ADDRESS Naval Air Systems Command Department of the Navy Washington, DC 20361		12. REPORT DATE February 1983
		13. NUMBER OF PAGES 44
14. MONITORING AGENCY NAME & ADDRESS(if different from Controlling Office)		15. SECURITY CLASS. (of this report) UNCLASSIFIED
		15a. DECLASSIFICATION/DOWNGRADING SCHEDULE

16. DISTRIBUTION STATEMENT (of this Report)

Approved for public release; distribution unlimited.

17. DISTRIBUTION STATEMENT (of the abstract entered in Block 20, if different from Report)

18. SUPPLEMENTARY NOTES

19. KEY WORDS (Continue on reverse side if necessary and identify by block number)

Tropical cyclone
Intensity forecast
Cloud spiral bands
Satellite analysis

20. ABSTRACT (Continue on reverse side if necessary and identify by block number)

An evaluation of the Spiral Linearization Technique (SLT) for digital tropical cyclone satellite images was performed to test the method's usefulness as a research tool. A stepwise multiple regression analysis, using SLT-derived parameters as the independent variables to predict current intensity and intensity change, was carried out for eastern Pacific hurricanes Dolores and Enrique, 1979. The spirals traced out by the cloud bands were found to have much larger inflow angles than those of the wind field, and it appears that the

((continued on reverse))

DD FORM 1 JAN 73 1473 EDITION OF 1 NOV 65 IS OBSOLETE S/N 0102-014-6601 |

UNCLASSIFIED

SECURITY CLASSIFICATION OF THIS PAGE (When Data Entered)

Block 20, Abstract, continued.

cloud band spirals can not be used as a tracer of the wind field spirals. The results of this project are sufficiently promising to warrant further investigation into the development of an objective technique to determine intensity changes utilizing parameters derived from digital infrared satellite images of tropical cyclones.

Contents

Acknowledgments

The author wishes to thank Mr. Roland Nagle, Dr. Ted Tsui and Mr. David H. Lee of NAVENVPREDRSCHFAC for many helpful suggestions and general guidance concerning programming and interpretation of the statistical output. Mr. Keith Nuttall of Systems and Applied Sciences Corporation was very helpful in the early stages of program modification. The author also appreciates the assistance of Mr. Ronald J. Sznaider and PH2 William Anderson in the photography, Ms. Winona Carlisle in manuscript word processing, and Mr. Stephen Bishop in editorial services.

1. INTRODUCTION

The current technique, recognized worldwide as the best available, for manually estimating tropical cyclone intensity based solely upon satellite imagery was developed by Vernon Dvorak (1975). Dvorak recognized the relationship of the cyclone's banding features (BF), and the areal extent and configuration of the central dense overcast (CDO) with the intensity of the storm. The technique gives a subjective, although systematic, estimate of the current intensity and the expected intensity change which is based upon a "T-number." The T-number which may range from T1 to T8, is an estimate of, where the cyclone "fits," in Dvorak's model of the chronological life cycle for "average" cyclones. The current intensity (CI) number is the same as the T-number when the cyclone closely follows the modeled amount of daily cloud feature change. Dvorak also shows a relationship between the CI number, wind speed and the minimum sea level pressure.

Upon examination of many hurricanes near the southeastern coast of the United States Senn and Hiser (1957) found that in general the spiral rainbands observed on radar closely resemble logarithmic spirals. They developed a method of determining the storm center using a logarithmic spiral overlay fitted to the spiral bands of the radar imagery. The accuracy of this method is comparable to that of conventional synoptic methods. Hughes (1952) combined data from a number of reconnaissance flights into large Pacific cyclones to obtain a generalized pattern of winds at low-levels (~1000 ft). He showed that the trajectories of the low-level inflow were logarithmic spirals, and computed averaged profiles of wind speed (both radial and tangential), relative vorticity and divergence. Lahiri (1981), under the assumption that the cloud spirals are coincident with the streamlines of the wind field, shows that the spiral constant, a, in the logarithmic spiral equation, $r = EXP[a\theta]$, is equal to the negative of the ratio of the radial and tangential velocities. He also shows that the ratio of divergence and relative vorticity are also equal to the negative of the spiral constant.

Infrared satellite image counts, from which equivalent blackbody temperatures of cloud tops are calculated, have been shown to contain meaningful information concerning intensity and intensity changes associated with tropical cyclones (Gentry et al., 1978). Latent heat released when air with high equivalent potential temperature ascends into the deep convective cells of tropical cyclones provides the primary energy source for the storms. The amount of latent heat released is related to the depth of the convective cells and their associated colder cloud tops, which ultimately is converted to kinetic energy by means of a complex nonlinear scale interaction conversion process. The time involved for this conversion from latent heat energy to available potential energy and then to kinetic energy is used to explain the observed time lag between the maximum convective activity and the maximum storm intensity.

The results of the previous studies, itemized above, suggest a physical relationship between satellite-observed cloud patterns associated with tropical cyclones and dynamic parameters known to be related to tropical cyclone intensity characteristics. As noted by Lahiri no direct method exists for objectively estimating the spiral cloud band parameters from satellite images.

The Spiral Linearization Technique (SLT) was devised to objectively analyze digital satellite image data so that cloud bands, which typically approximate spiral shapes, could be more directly related to tropical cyclone characteristics, such as intensity. Estimates of tropical cyclone intensity, intensity changes, movement, and position are currently determined subjectively from satellite images and other forecast aids. The accuracy of these estimates is highly subjective and dependent on the analyst's experience. The development of objective techniques to analyze and extract information from digital satellite data of tropical cyclones is essential.

2. THE CURRENT SLT

The Spiral Linearization Technique software was designed to utilize the Satellite-Data Processing and Display System's (SPADS) unique capabilities of allowing interactive digital image processing (Schramm, Zeleny, Nagle, and Weinstein, 1982). The SLT consists of the following three main steps. The flow diagram for the SLT is shown in Figure 1.

2.1 IMAGE PREPARATION (SATMG)

Upon selecting and displaying the desired tropical cyclone image, the user must enhance the image so that the dominant spiral feature is isolated. The center of the spiral feature is then defined by positioning a cursor on the spiral center by means of the graph pen/pad or console entry. Then subsetting by means of an inner and outer radii is performed next. The inner radius is chosen so that the CDO is encompassed to avoid unnecessary pixel transformations in step 2. The outer radius is set to include the entire spiral band. This is shown in Figure 2.

2.2 TRANSFORMATION TO SPIRAL COORDINATES (SLTMG)

The preprocessed image can be simultaneously transformed to any or all of the four spiral types which include archimedian, hyperbolic, logarithmic and parabolic spirals. The transformed image(s) is displayed and examined to see if the proper zero degree reference angle is acceptable. The zero degree reference angle is the starting theta (θ) for the transformation from x,y space to r,θ space. The above scheme is illustrated in Figure 3. The transformation algorithm has been modified to allow for a variable offset radius, R_O, defined by the user, which allows for a more realistic spiral pattern configuration due to the fact that spiral cloud bands appear to be spiraling into the eyewall (of radius R_O) rather than into an absolute center point. The effect of an offset radius in the spiral configuration is shown in Figure 4.

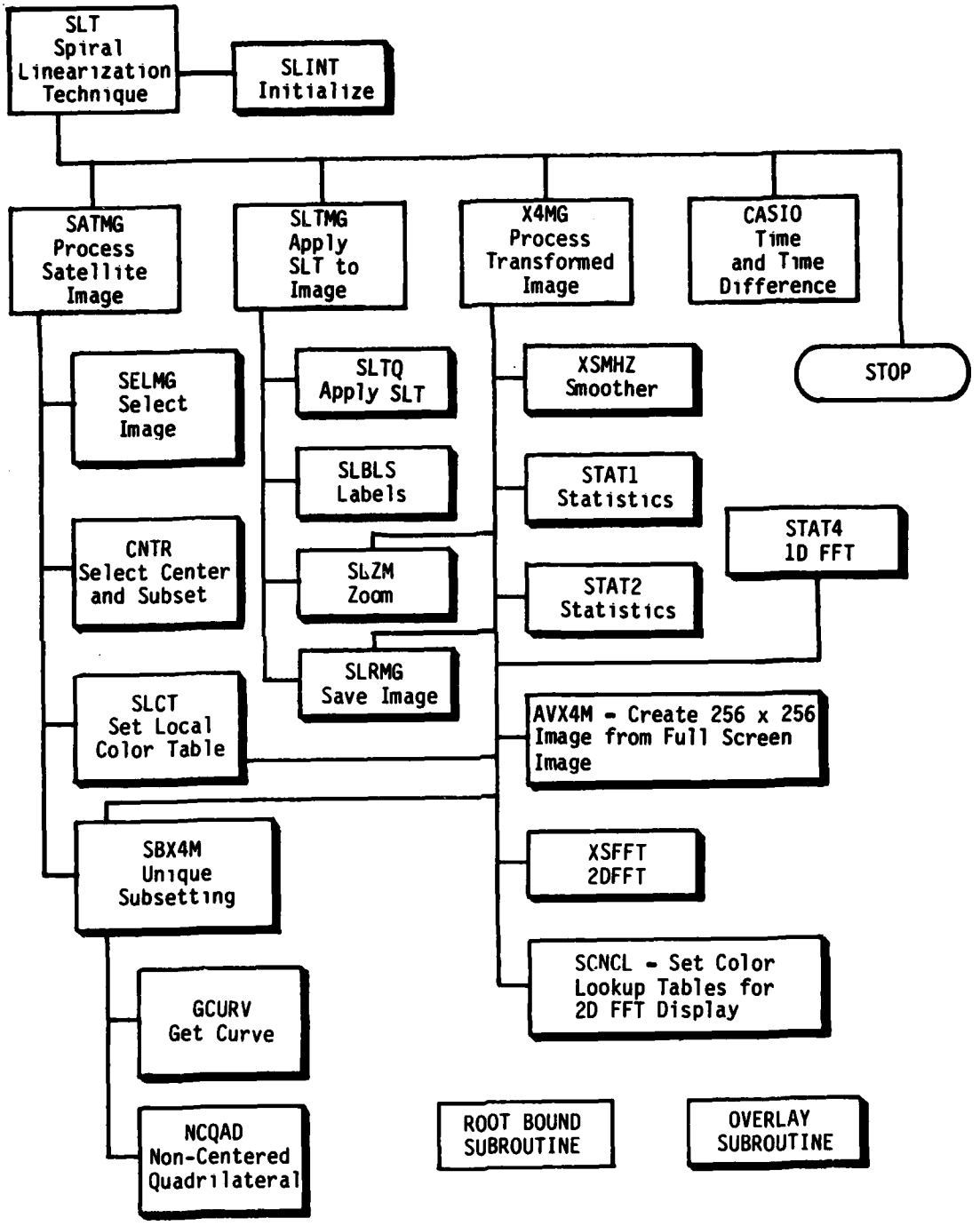

Figure 1. Functional flow diagram for the SLT program.

Figure 2. Subsetting by inner and outer radii before transformation to spiral coordinates.

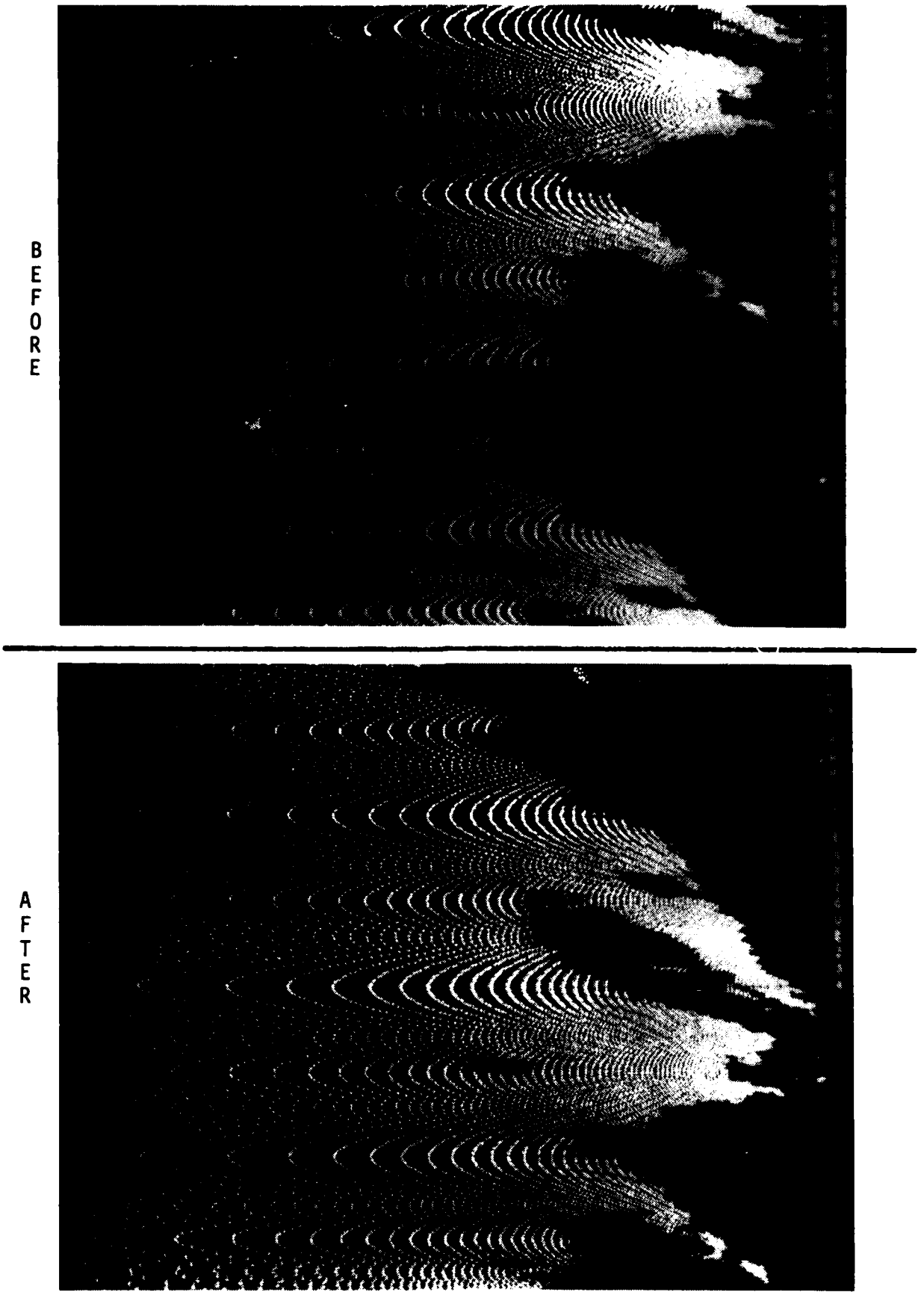

Figure 3. Setting a proper zero degree reference angle.

Logarithmic Spirals: $R = R_0 + EXP(a\theta)$

$a = 0.50$
$R_0 = 0.0$

$a = 0.50$
$R_0 = 30.0$

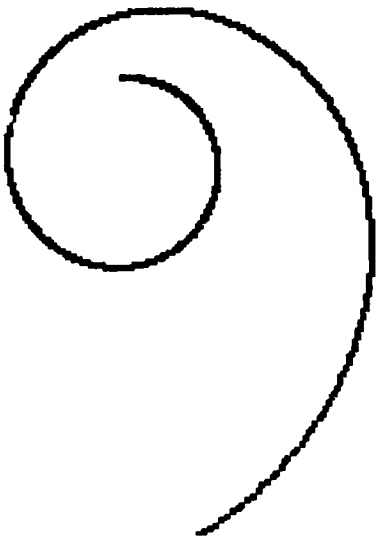

Figure 4. The effect of an offset radius on the configuration of the logarithmic spiral.

2.3 PROCESSING THE TRANSFORMED IMAGE (X4MG)

The transformed image must be processed further prior to entering the statistics routine. All pixels of the image contained within the inner and outer radii have been transformed, leaving cloud features not related to the spiral band remaining in the image. The image must be further subsetted so that only the pixels constituting the spiral band are retained. Once this is accomplished the statistical evaluation of the spiral band can begin. The "goodness of fit" of the observed spiral band to the given spiral type is measured by the linearity of the transformed spiral band. The statistics routine computes a linear least squares line, correlation coefficient, sum of the errors, root mean square error, mean error as well as the coefficient of variation. The SLT slope of the linear least squares line is then correlated with the known spiral constants of several perfect logarithmic spiral images generated with the SLTVY program, and is found to obey a power law formula. The equation is of the form, $Y = AX^B$, where Y is the spiral constant, X is the SLT least squares slope, and A and B are constants with values of 4.5838 and -0.99214, respectively. This relationship is illustrated in Figure 5. The logarithmic spiral constant can be shown to be related to the inflow angle, α, with the relationship,

$$\text{TAN}\,\alpha = \frac{1}{r}\frac{dr}{d\theta} = a. \qquad (1)$$

The relationship between the inflow angle and the SLT least squares slope is shown in Figure 6. Logarithmic spirals with offset radii obey a slightly modified inflow angle relationship, i.e.,

$$\text{TAN}\,\alpha = \frac{1}{r}\frac{dr}{d\theta} = a\left(1 - \frac{R_o}{r}\right). \qquad (2)$$

From this equation it is seen that for radii near the offset radius, the inflow angle approaches zero, while for large radii, $r >> R_o$, the inflow angle approaches that of a spiral with offset radius equal to zero

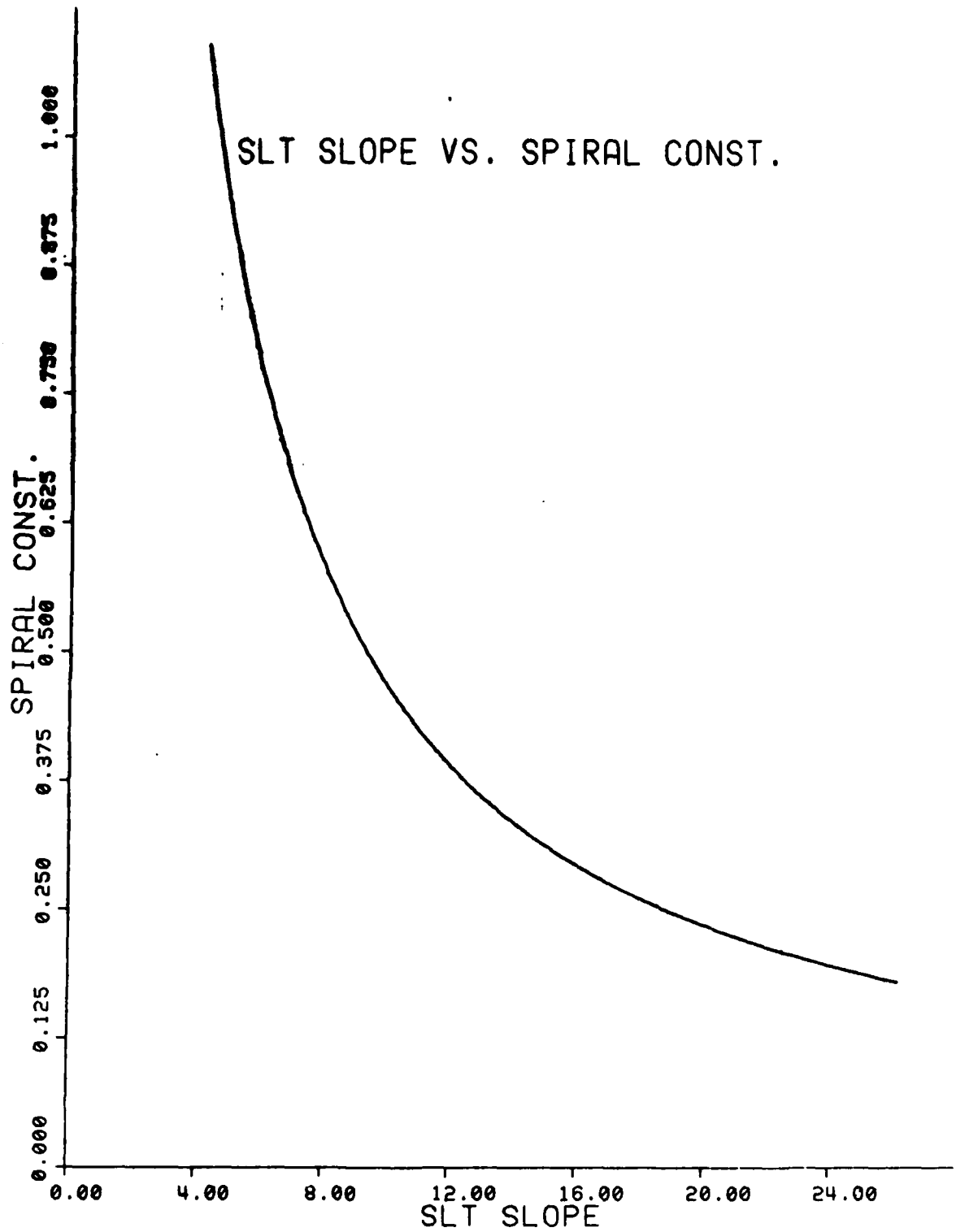

Figure 5. SLT slope vs. spiral constant

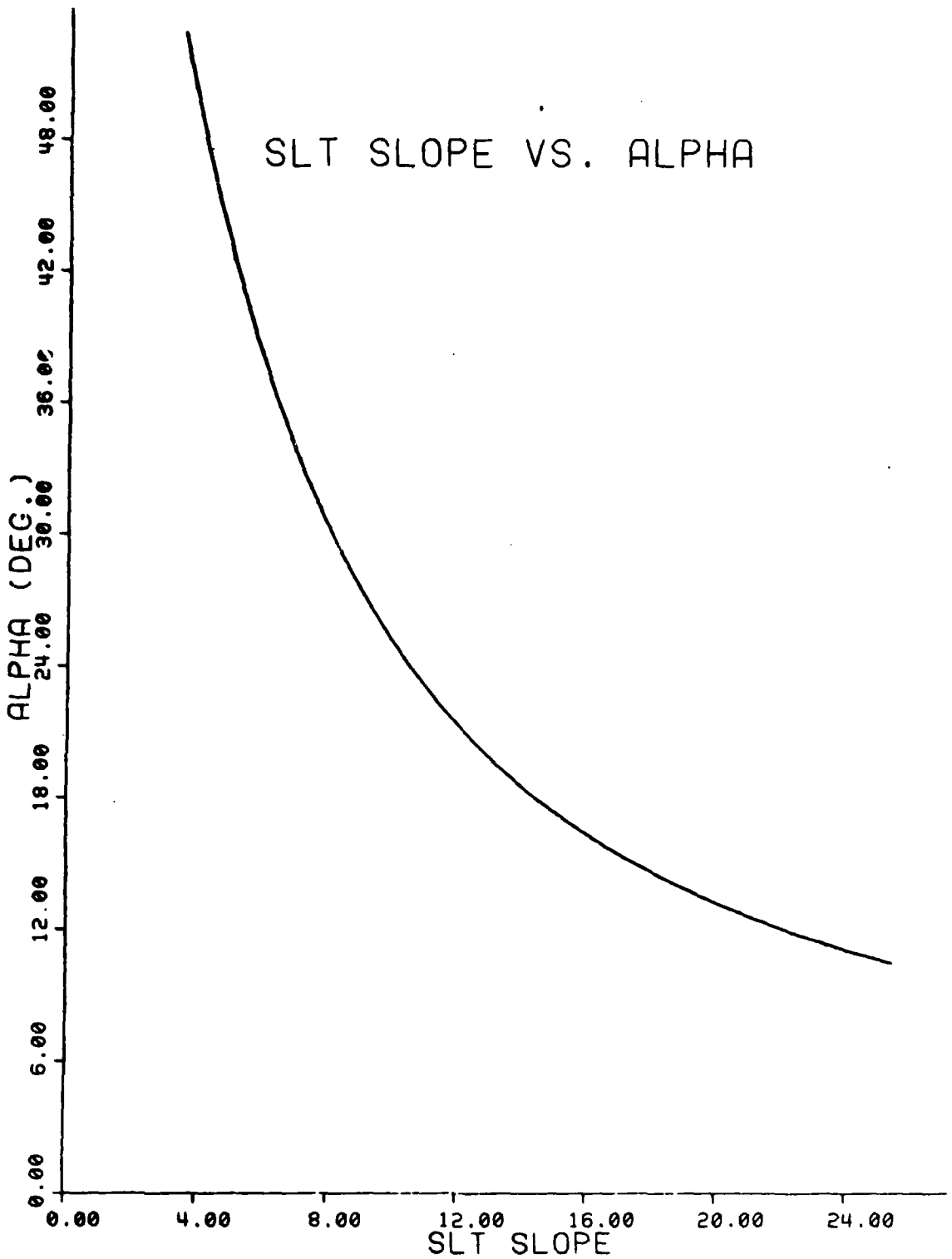

Figure 6. SLT slope vs. inflow angle alpha.

The calculation of a one-dimensional Fast-Fourier-Transform (FFT) of the average theta value at each radius (in pixel units) along the least squares line is the next SLT option. A graphical plot of the power spectra values (the sum of the squared real and imaginary FFT coefficients) vs. wave number can be constructed if desired. Inferences on cloud spacing and orientation can be made by examining the power spectra coefficients, provided the transformed spiral band is free from geometric distortion.

The final processing option is the calculation of a two-dimensional FFT of the entire spiral band. The SLT has the capability of displaying the magnitude of the FFT coefficients in image format. To compensate for the rapid decrease of the image spectra with increasing frequencies, the displaying of the natural log of one plus the magnitude of the FFT coefficients, i.e.,

$$D(u,v) = \log_e (1 + |F(u,v)|), \qquad (3)$$

greatly facilitates the visual interpretation of the two-dimensional FFT display (Gonzalez and Wintz, 1977) as illustrated in Figure 7. A plot of the radially averaged profile of the two-dimensional FFT power spectra coefficients was also devised. The DC component is used as the center. This will give a linear representation of the behavior of the mean wave numbers in the two-dimensional FFT result.

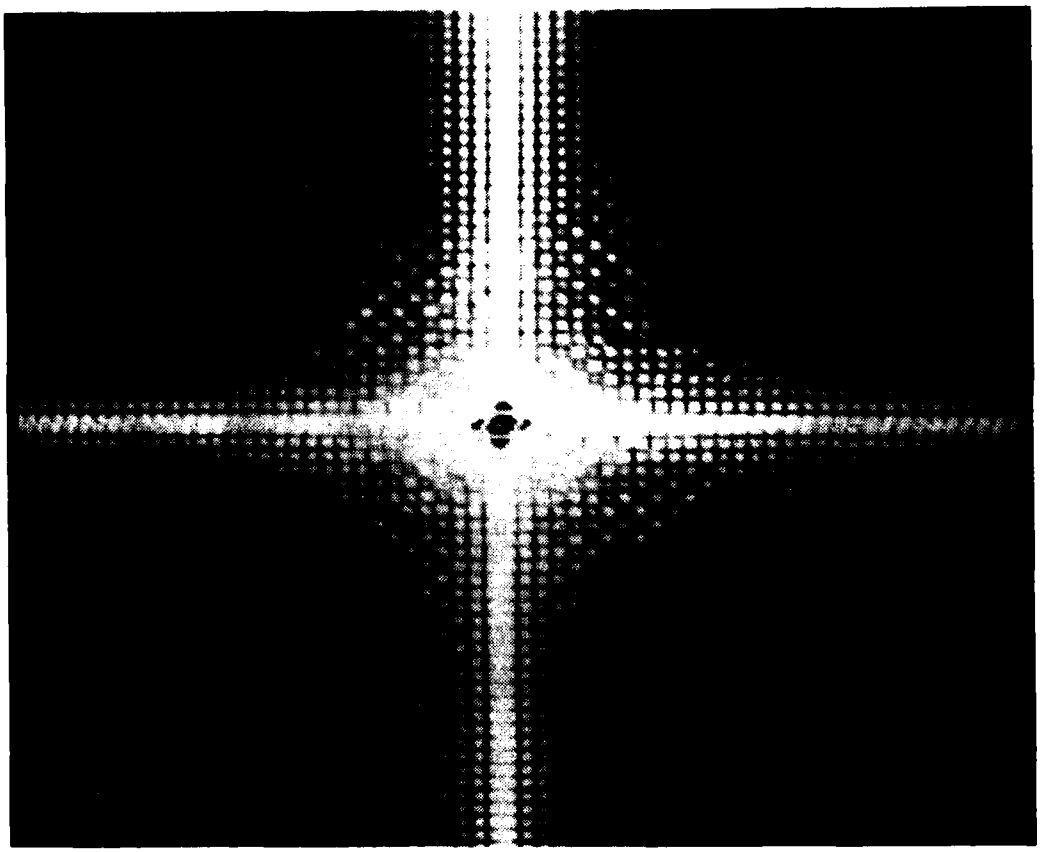

Figure 7. Two-dimensional FFT image display with DC component at center.

3. DATA AND ANALYSIS

The dependent data set consisted of two mile infrared satellite images from the geosynchronous GOES WEST satellite. Cyclonic storm intensity estimates and positioning were given by Gunther (1980) using the Dvorak technique of satellite cyclone analysis (Dvorak, 1975). This data set was supplemented by Fleet Numerical Oceanography Center's archived tropical cyclone data set which contain maximum wind speed at six hour intervals for the life cycle of each storm.

Two tropical cyclone cases were selected from the limited IR image sets, and upon the availability of continuous wind and image data. The two cases chosen were eastern Pacific hurricanes Dolores and Enrique. Descriptive life histories of the storms will follow.

3.1 HURRICANE DOLORES, 17-23 JULY, 1979

The sixth tropical disturbance of the 1979 season originated approximately 350 n mi south of the Guatemalan coast and began a westward progression at about 10 kt on 14 July. Intensifying cyclonic circulation by 0600 GMT 17 July was evident and the disturbance was upgraded to a tropical depression. The rate of intensification increased and by 1800 GMT the same day the depression was upgraded to tropical storm Dolores near 11.2^{o}N and 107.0^{o}W. Sea surface temperatures of 29^{o}C were conducive to further rapid development as the storm moved around the southwest edge of an upper level anticyclone centered over Baja, California. Wind speeds increased to 65 kt by 1800 GMT 18 July. The initial satellite image was for 1345 GMT 18 July and was the first of twenty-one images analyzed, the last being at 2145 GMT 22 July. Wind speeds continued to increase and reached their maximum intensity of 105 kt by 0000 GMT on 21 July. Dolores continued to move northwest and began to weaken over cooler (25^{o}C) water and was downgraded to a tropical storm by 0000 GMT 22 July near 20.3^{o}N, 121.8^{o}W. By 0000 GMT 23 July winds had decreased to less than 30 kt. Figure 8 shows Dolores at maximum intensity

Figure 8. Hurricane Dolores near maximum intensity (105 kt) at 0215 GMT 21 July 1979.

3.2 HURRICANE ENRIQUE, 17-24 AUGUST 1979

Nearly a month elapsed before the next tropical disturbance began significant development near 11°N, 107°W. Sea surface temperatures of 30°C favored continued development as the disturbance moved westward. At 1800 on the 17th the disturbance was upgraded to a tropical depression and six hours later was upgraded to tropical storm Enrique near 11.2°N, 114.9°W. Enrique reached hurricane strength by 0000 GMT 19 August near 12.8°N, 119.0°W, but then weakened as the storm moved over 27°C water. Enrique was downgraded to a tropical storm with winds of 55 kt on the 21st. By 1700 GMT on the 21st Enrique again reached hurricane strength and began a rapid intensification. By 0000 GMT on the 22nd wind speeds reached 110 kt and reached maximum intensity of 125 kt by 1200 GMT. Satellite images beginning at 1415 GMT 21 August and ending at 0415 GMT 23 August, for a total of nineteen images, were analyzed via the SLT. Moving northwestward, Enrique began to move over cooler water and was downgraded to a tropical storm by 1200 GMT 23 August near 20.4°N, 132°W. Enrique's final position was 21.3°N, 135.8°W at 1800 GMT on the 24th when little more than a low-level vortex remained. Figure 9 shows Hurricane Enrique near maximum intensity.

3.3 THE CASE STUDIES

While carrying out the case studies, it became apparent that the logarithmic spiral type best conformed to the spiral configurations evident in the satellite data, and, in order to save computation time, was the only spiral type employed. If a combined cylindrical vortex and sink are considered, then the stream function is

$$\psi = -m\theta + \kappa \log_e r, \qquad (4)$$

where m/κ is the spiral constant for the logarithmic spirals traced out by constant values of ψ (Milne-Thompson, 1960). However, the selection of the logarithmic spiral type pre-empted: (a) applying the one-dimensional FFT to the subsetted transformed

Figure 9. Hurricane Enrique near maximum intensity (125 kt) at 1415 GMT 22 July 1979.

spiral bands and (b) deducing the spectrum of cloud sizes due to the distortion of the transformed image caused by the nature of the transformation algorithm.

The approach during the case studies was to process each of the images with the SLT in an identical manner. While some subjectivity was entered into the analysis by the selection of enhancement limits, band to evaluate, etc., the storms were treated identically after the preprocessing of the image was accomplished. To keep minor statistical variations to a minimum, an arbitrary inner radius of 30 pixels was chosen based upon preliminary experiments.

The SLT parameters which were recorded for each image are: maximum IR count in storm, maximum IR count in the spiral band, minimum IR count in band, average IR count in band, and the spiral inflow angle. The minimum IR count in the band was the most subjectively defined parameter as it was chosen by incrementing the lower enhancement limit until the spiral band became "prominent." The average IR count in band was defined as the mean value of the maximum and minimum values rather than an actual mean of the pixel counts comprising the band. The spiral inflow angle recorded was that for large radii ($R >> R_0$).

The maximum wind speed data was plotted vs. time and the wind speed values at the times of the satellite images were interpolated from these plots. A three point running mean was applied to the SLT parameters to smooth some of the variance out of the data. SLT data for both Enrique and Dolores vs. maximum wind speed is shown in Table 1. The rate of intensity change was calculated using a forward difference scheme with the user supplying the initial maximum wind speed and subsequently using the above maximum wind speeds. The time increment was the time between satellite images. The rate of intensity change vs. the SLT data for Dolores and Enrique are shown in Table 2.

Table 1. SLT-derived parameters for Dolores and Enrique vs. maximum wind speed.

DOLORES

IRMAX	IBMAX	IBAV	IBMN	a	ALPHA	VMAX
228.0	228.0	218.0	208.0	.575	36.3	44.000
230.0	222.0	210.0	197.3	.641	32.6	48.000
230.7	218.3	204.5	190.0	.610	31.4	66.000
230.3	213.3	198.2	182.3	.639	32.5	66.000
226.0	215.3	201.8	188.3	.638	32.5	66.000
225.3	214.3	203.0	192.3	.598	30.7	68.000
223.7	213.0	202.7	192.3	.558	29.0	70.000
224.7	212.0	201.8	191.7	.581	30.0	80.000
222.7	203.7	191.3	179.0	.517	27.0	94.000
223.7	205.3	192.0	178.7	.588	29.8	98.000
223.7	204.0	186.3	168.7	.505	26.1	100.000
223.7	210.3	190.8	174.7	.647	32.3	102.000
223.0	206.7	187.5	169.7	.501	26.0	104.000
221.7	204.3	185.8	167.7	.606	30.6	98.000
220.0	194.0	176.0	155.0	.509	26.6	96.000
218.0	196.0	176.7	156.0	.675	33.6	92.000
218.0	200.0	181.0	161.7	.583	29.7	90.000
217.0	208.0	191.7	175.0	.643	32.2	88.000
216.7	200.7	189.8	172.7	.569	29.5	84.000
215.3	205.7	166.7	167.3	.552	28.6	76.000
216.0	206.5	184.0	161.0	.504	26.5	70.000

ENRIQUE

223.0	191.0	181.0	171.0	.678	31.8	56.000
222.7	189.7	180.5	171.3	.641	32.4	58.000
222.7	194.3	186.2	178.0	.688	34.6	60.000
223.0	202.7	193.8	185.0	.778	38.2	62.000
222.7	206.8	199.0	192.0	.700	35.1	66.000
222.3	207.7	199.5	191.3	.665	33.3	78.000
222.0	206.0	197.2	188.3	.700	34.5	83.000
221.3	207.7	192.8	178.0	.683	33.8	96.000
221.3	204.7	184.8	165.0	.579	29.1	105.000
219.7	203.3	183.3	163.3	.409	22.3	112.000
218.7	198.7	180.5	162.3	.451	24.0	124.000
216.7	202.7	185.5	168.3	.588	30.0	125.000
216.3	200.7	183.2	165.7	.759	36.9	125.000
215.7	199.0	180.5	162.0	.734	35.9	125.000
215.0	189.7	172.7	155.7	.664	33.1	125.000
213.3	192.0	171.3	150.7	.562	29.3	125.000
210.3	1914.0	172.5	151.0	.589	30.4	124.000
209.7	200.7	177.8	155.0	.699	34.6	117.000
209.0	200.5	178.3	156.0	.757	36.8	104.000

All SLT parameters are 3 pt. running means VMAX (kt), ALPHA (deg)

Table 2. SLT-derived parameters for Dolores and Enrique vs. rate of intensity change.

DOLORES

IRMAX	IBMAX	IBAV	IBMN	a	ALPHA	RIC
228.0	228.0	218.0	208.0	.575	36.3	2.000
230.0	222.0	210.0	197.3	.641	32.6	1.667
230.7	218.3	204.5	190.0	.610	31.4	1.071
230.3	213.3	198.2	182.3	.639	32.5	.000
226.0	215.3	201.8	188.3	.638	32.5	.000
225.3	215.3	203.8	192.3	.598	30.7	.556
223.7	213.0	202.7	192.3	.558	29.0	.833
224.7	212.0	201.8	191.7	.581	30.0	2.083
222.7	203.7	191.3	179.0	.517	27.0	2.917
223.7	205.3	192.0	178.7	.588	29.8	1.667
223.7	204.0	186.3	168.7	.505	26.1	.417
223.7	210.3	190.8	174.7	.647	32.3	.833
223.0	206.7	187.5	169.7	.501	26.0	.417
221.7	204.3	185.8	167.7	.606	30.6	-1.250
220.0	194.0	176.0	155.0	.509	26.6	-.833
218.0	196.0	176.7	156.0	.675	33.6	-1.667
218.0	200.0	181.0	161.7	.583	29.7	-.833
217.0	208.0	191.7	175.0	.643	32.2	-.417
216.7	206.7	189.8	172.7	.569	29.5	-1.667
215.3	205.7	186.7	167.3	.552	28.6	-2.222
216.0	206.5	184.0	161.0	.504	26.5	-5.000

ENRIQUE

223.0	191.0	181.0	171.0	.670	31.8	.833
222.7	189.7	180.5	171.3	.641	32.4	.833
222.7	194.3	186.2	178.0	.688	34.6	.833
223.0	202.7	193.8	185.0	.778	38.2	.833
222.7	206.0	199.0	192.0	.700	35.1	1.667
222.3	207.7	199.5	191.3	.665	33.3	5.000
222.0	206.0	197.2	188.3	.700	34.5	2.083
221.3	207.7	192.8	178.0	.683	33.8	5.417
221.3	204.7	184.8	165.0	.579	29.1	3.750
219.7	203.3	183.3	163.3	.409	22.3	2.917
218.7	198.7	180.5	162.3	.451	24.0	2.500
216.7	202.7	185.5	168.3	.588	30.0	.417
216.3	200.7	183.2	165.7	.759	36.9	.000
215.7	199.0	180.5	162.0	.734	35.9	.000
215.0	189.7	172.7	155.7	.664	33.1	.000
213.3	192.0	171.3	150.7	.562	29.3	.000
210.3	194.0	172.5	151.0	.589	30.4	-.278
209.7	200.7	177.8	155.0	.699	34.6	-2.917
209.0	200.5	178.3	156.0	.757	36.8	-5.417

3 pt. running means RIC (kt/Hr)

3.4 DEVELOPMENT OF PREDICTIVE EQUATIONS

The equations developed rely solely upon IR satellite information to predict maximum wind speeds and rate of intensity changes. A stepwise multiple regression was performed, and depending upon the significance level for deleting variables, retained either three or four independent variables. The three variables retained were: maximum IR-storm (IRMAX), maximum IR-band (IBMAX), and the spiral inflow angle (ALPHA). The fourth independent variable, when used, was the average IR-band (IBAV). Separate regression equations were developed for both Dolores and Enrique.

The equations developed to predict the maximum wind speeds work well with three independent variables. The addition of the fourth predictor only accounts for an additional 6% of the explained variance, in the case of Enrique, while for Dolores there is virtually no change in the percent variance explained. The analysis of variance tables for both the three and four independent variable cases are shown in Table 3 for Dolores and Table 4 for Enrique. The regression equation for Dolores using three independent variables is,

$$V_{max} = B0 + B1*IRMAX + B2*IBMAX + B3*ALPHA \quad (5)$$

where B0 = 352.4, B1 = 0.6148, B2 = 1.869, and B3 = -0.6001 are the linear regression coefficients. The four variable equation is,

$$V_{max} = B0 + B1*IRMAX + B2*IBMAX + B3*IBAV + B4*ALPHA \quad (6)$$

where B0 = 322 3, B1 = 0.6816, B2 = -1.543, B3 = -0.2702 and B4 = -0.6188. Plots of the predicted vs. observed maximum wind speeds via the three and four variable regression equations for Dolores are shown in Figures 10 and 11.

Table 3. Analysis of variance table for Dolores (maximum wind speed).

THREE INDEPENDENT VARIABLES

Source of Variation	Degrees of Freedom	Sums of Squares	Mean Squares	F-Value	P (Exceeding F under HO)
Regression	.30000E 01	.41479E 04	.13826E 04	.11841E 02	.19819E-03
Residual	.17000E 02	.19850E 04	.11677E03		
Total	.20000E 02	.61330E 04			

** GOODNESS OF FIT ESTIMATES **

Percentage of Variance Explained = .67633E 02
Standard Deviation of Residuals = .10806E 02
As a Percentage of Response Mean = .13348E 02

FOUR INDEPENDENT VARIABLES

Regression	.40000E 01	.41578E 05	.10394E 04	.84199E 02	.74351E-03
Residual	.16000E 02	.19752E 04	.12345E 03		
Total	.20000E 02	.61330E 04			

** GOODNESS OF FIT ESTIMATES **

Percentage of Variance Explained = .67794E 02
Standard Deviation of Residuals = .11111E 02
As a Percentage of Response Mean = .13725E 02

Table 4. Analysis of variance table for Enrique (maximum wind speed).

THREE INDEPENDENT VARIABLES

Source of Variation	Degrees of Freedom	Sums of Squares	Mean Squares	F-Value	P (Exceeding F under HO)
Regression	.30000E 01	.94710E 04	.31570E 04	.12075E 02	.27877E-03
Residual	.15000E 02	.39217E 04	.26145E 03		
Total	.18000E 02	.13393E 05			

** GOODNESS OF FIT ESTIMATES **

Percentage of Variance Explained = .70718E 02
Standard Deviation of Residuals = .16169E 02
As a Percentage of Response Mean = .16429E 02

FOUR INDEPENDENT VARIABLES

Regression	.40000E 01	.10238E 05	.25534E 04	.11358E 02	.25564E-03
Residual	.14000E 02	.31549E 04	.22535E 03		
Total	.18000E 02	.13393E 05			

** GOODNESS OF FIT ESTIMATES **

Percentage of Variance Explained = .76443E 02
Standard Deviation of Residuals = .15012E 02
As a Percentage of Response Mean = .15253E 02

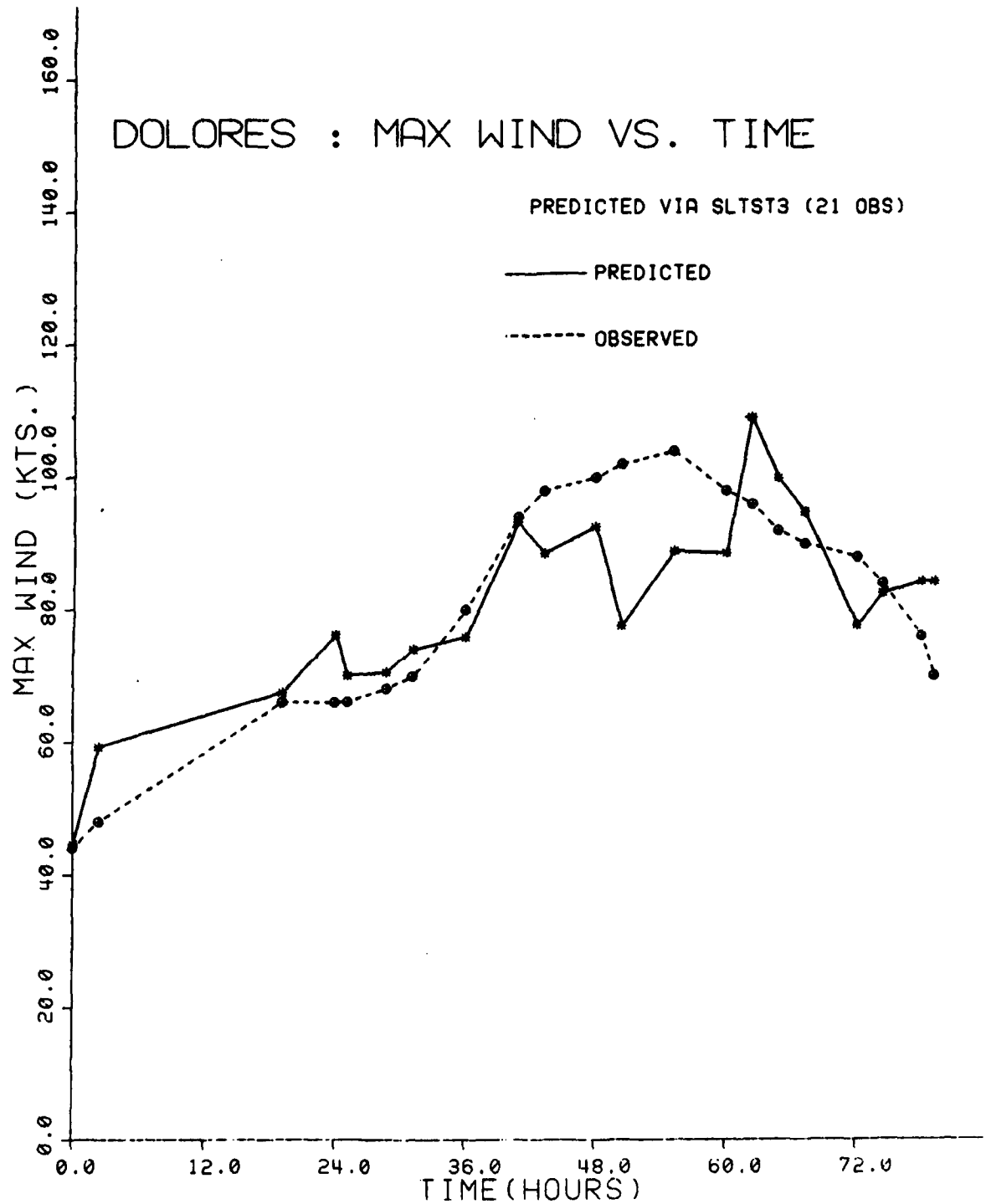

Figure 10. Predicted and observed maximum wind speeds for Dolores using three independent variables.

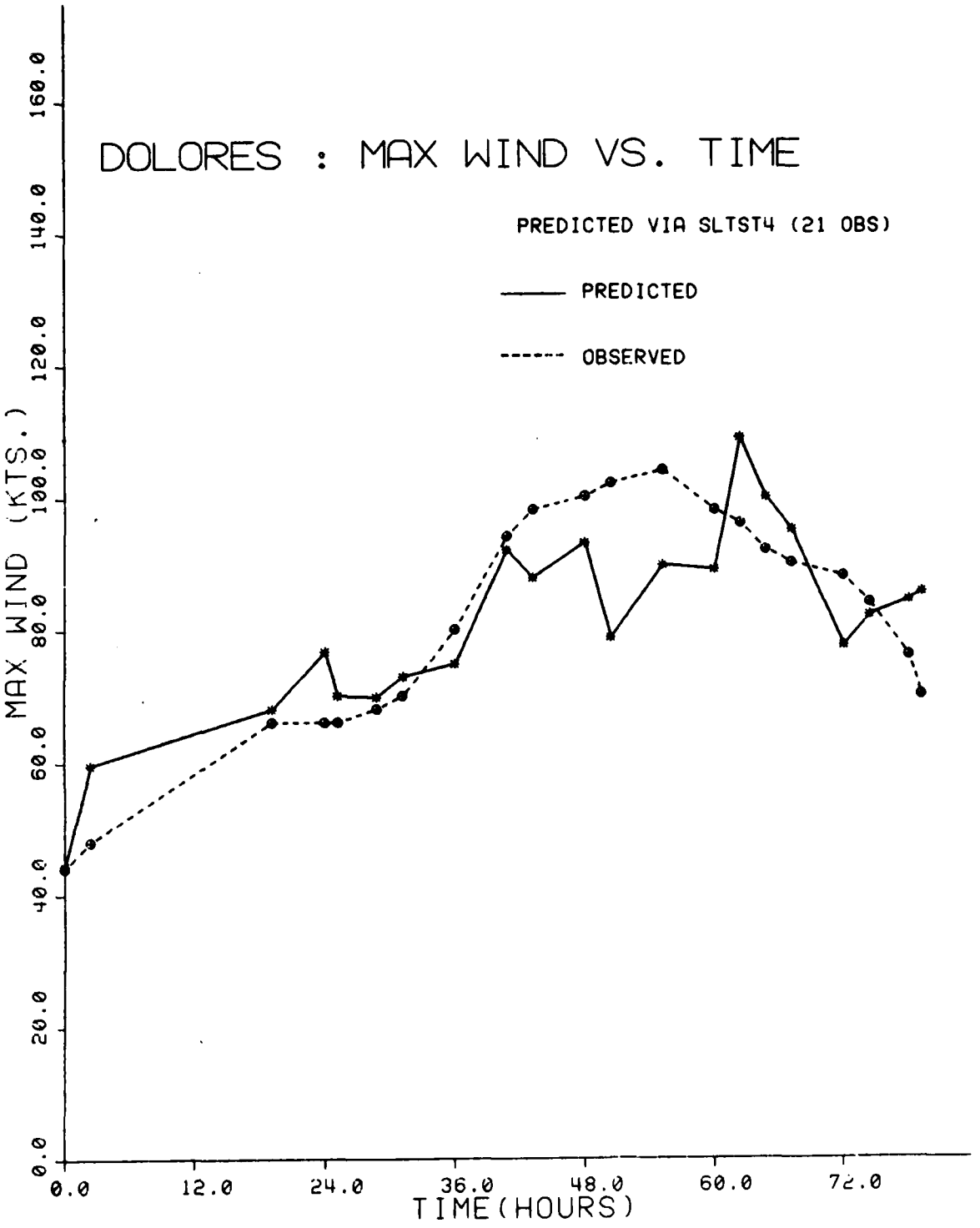

Figure 11. Predicted and observed maximum wind speeds for Dolores using four independent variables.

The regression equation for Enrique using three independent variables is of the same form as for Dolores, except the regression coefficients have the following values: B0 = 968.1, B1 = -4.46, B2 = 0.8934 and B3 = -2.354. The four variable equation has coefficients with the following values: B0 = 277.2, B1 = -1.397, B2 = 3.583, B3 = 3.038 and B4 = -0.8751. Plots of the predicted vs. observed maximum wind speeds via the three and four variable equations for Enrique are shown in Figures 12 and 13.

The equations developed to predict rate of intensity changes (RIC) required the inclusion of four variables to explain more than 50% of the variance in the case of Dolores, while there wasn't a significant difference in the percent of variance explained when either three or four variables were used in the case of Enrique. The analysis of variance tables for both the three and four variable cases are shown in Table 5 for Dolores and Table 6 for Enrique.

The regression equation for Dolores using three independent variables is,

$$RIC = B0 + B1*IRMAX + B2*IBMAX + B3*ALPHA \quad (7)$$

where B0 = -61.29, B1 = 0.2584, B2 = 0.0147 and B3 = 0.029. The four variable equation is,

$$RIC = B0 + B1*IRMAX + B2*IBMAX + B3*IBAV + B4*ALPHA \quad (8)$$

where B0 = -21.22, B1 = 0.1694, B2 = -0.4194, B3 = 0.3599 and B4 = 0.054.

The regression equations for Enrique are of the same form in both cases. The coefficients for the three variable equation are: B0 = -90.28, B1 = 0.34, B2 = 0.1233 and B3 = -0.2275; while for the four variable equation they are as follows: B0 = -108.6 B1 = 0.4213, B2 = 0.1947, B3 = -0.0805 and B4 = -0.1883. Plots of the predicted vs. observed intensity changes via the three and four variable regression equations for Dolores and Enrique are hown in Figures 14-17.

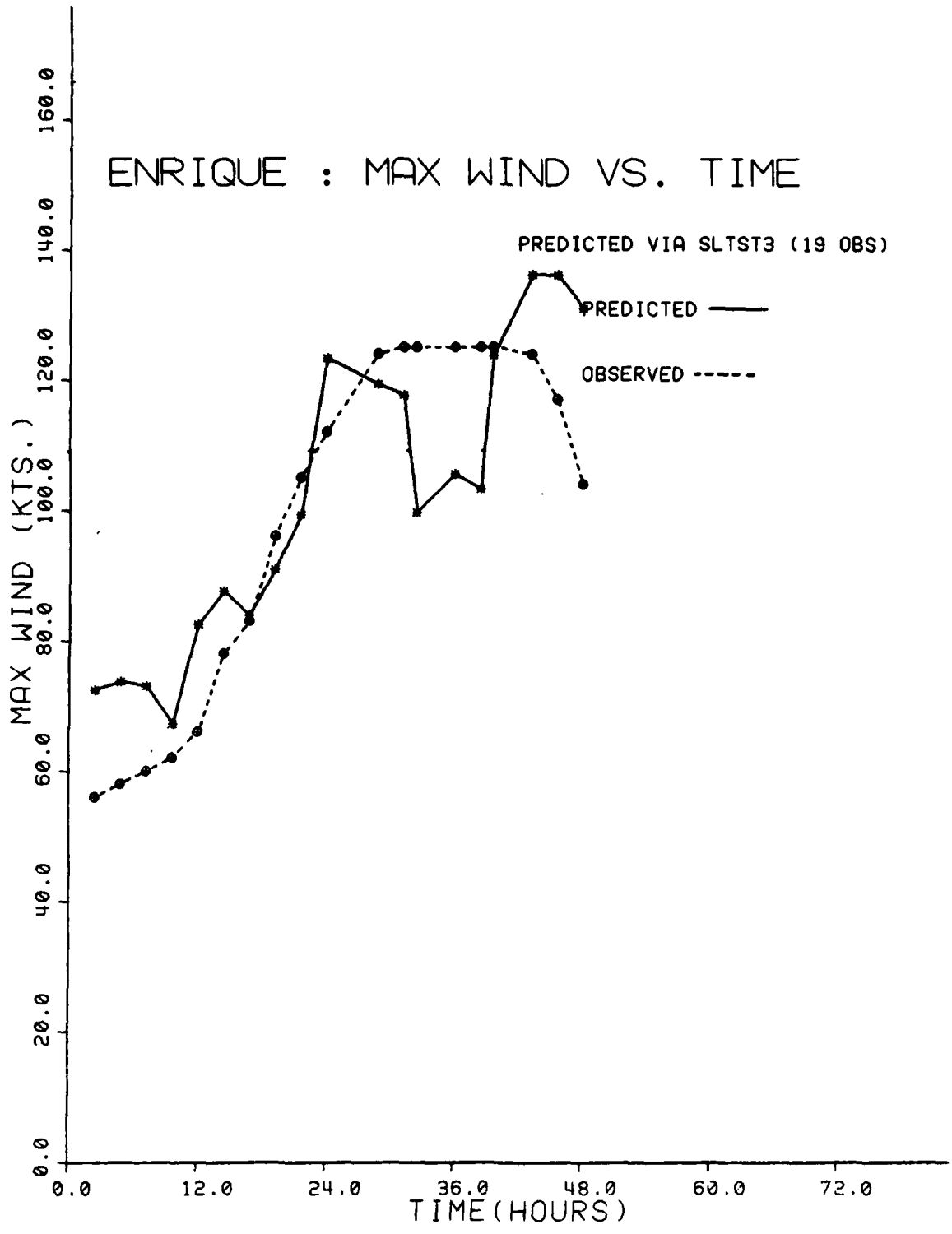

Figure 12. Predicted and observed maximum wind speeds for Enrique using three independent variables.

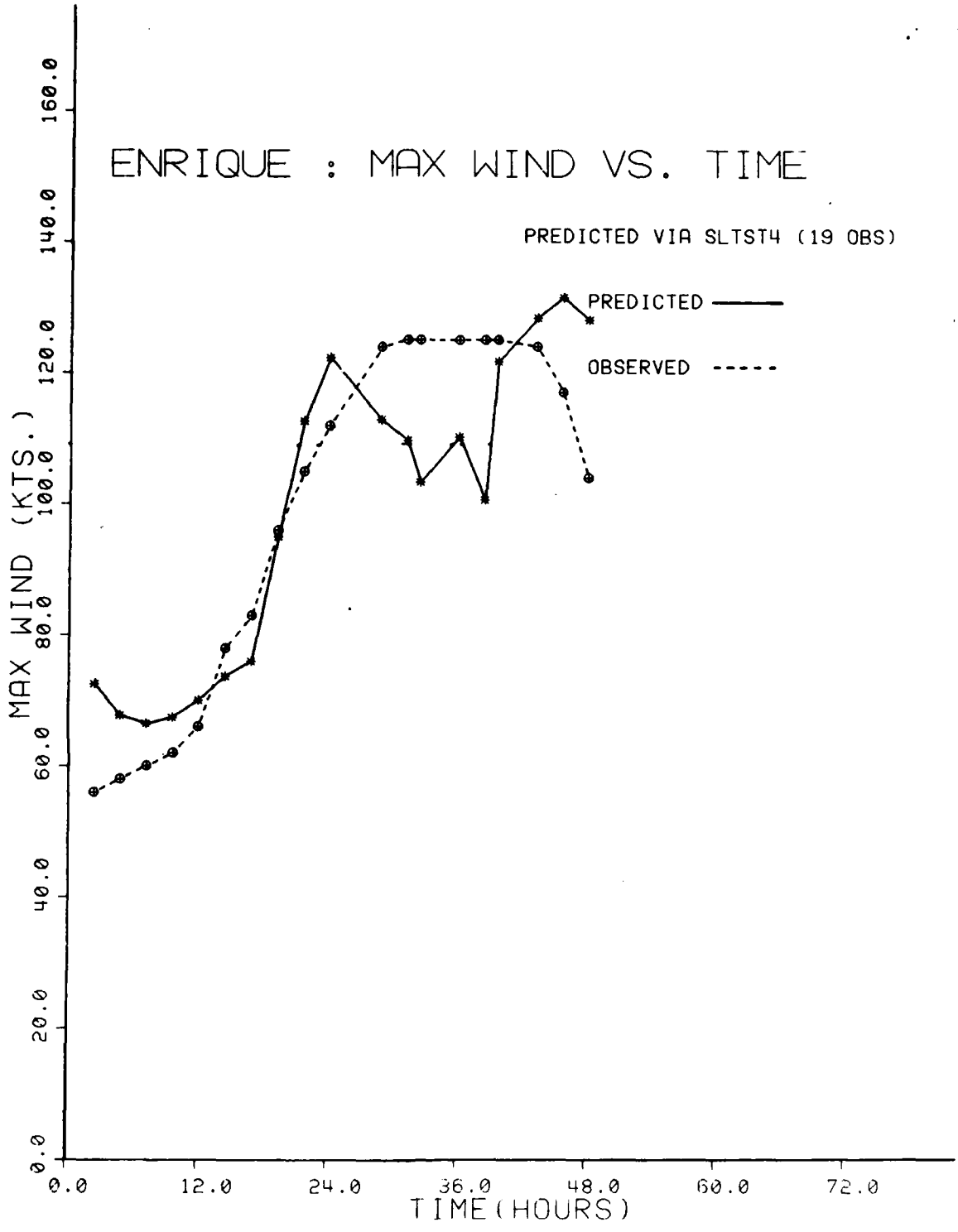

Figure 13. Predicted and observed maximum wind speeds for Enrique using four independent variables.

Table 5. Analysis of variance table for Dolores (rate of intensity change).

THREE INDEPENDENT VARIABLES

Source of Variation	Degrees of Freedom	Sums of Squares	Mean Squares	F-Value	P (Exceeding F under H0)
Regression	.30000E 01	.35974E 02	.11991E 02	.51055E 02	.10610E-01
Residual	.17000E 02	.39928E 04	.23487E 01		
Total	.20000E 02	.75901E 02			

** GOODNESS OF FIT ESTIMATES **

Percentage of Variance Explained = .47395E 02
Standard Deviation of Residuals = .15325E 01
As a Percentage of Response Mean = .12513E 04

FOUR INDEPENDENT VARIABLES

Regression	.40000E 01	.53414E 02	.13354E 02	.95012E 01	.39351E-03
Residual	.16000E 02	.22487E 04	.14055E 01		
Total	.20000E 02	.75901E 02			

** GOODNESS OF FIT ESTIMATES **

Percentage of Variance Explained = .70373E 02
Standard Deviation of Residuals = .11855E 01
As a Percentage of Response Mean = .96796E 03

Table 6. Analysis of variance table for Enrique (rate of intensity change).

THREE INDEPENDENT VARIABLES

Source of Variation	Degrees of Freedom	Sums of Squares	Mean Squares	F-Value	P (Exceeding F under HO)
Regression	.30000E 01	.83833E 02	.279744 02	.14271E 02	.11474E-03
Residual	.15000E 02	.29373E 02	.19582E 01		
Total	.10000E 02	.11321E 03			

** GOODNESS OF FIT ESTIMATES **

Percentage of Variance Explained = .74054E 02
Standard Deviation of Residuals = .13993E 01
As a Percentage of Response Mean = .14394E 03

FOUR INDEPENDENT VARIABLES

Regression	.40000E 01	.84372E 02	.21093E 02	.10242E 02	.43231E-03
Residual	.14000E 02	.28834E 02	.20596E 01		
Total	.18000E 02	.11321E 03			

** GOODNESS OF FIT ESTIMATES **

Percentage of Variance Explained = .74530E 02
Standard Deviation of Residuals = .14351E 01
As a Percentage of Response Mean = .14762E 03

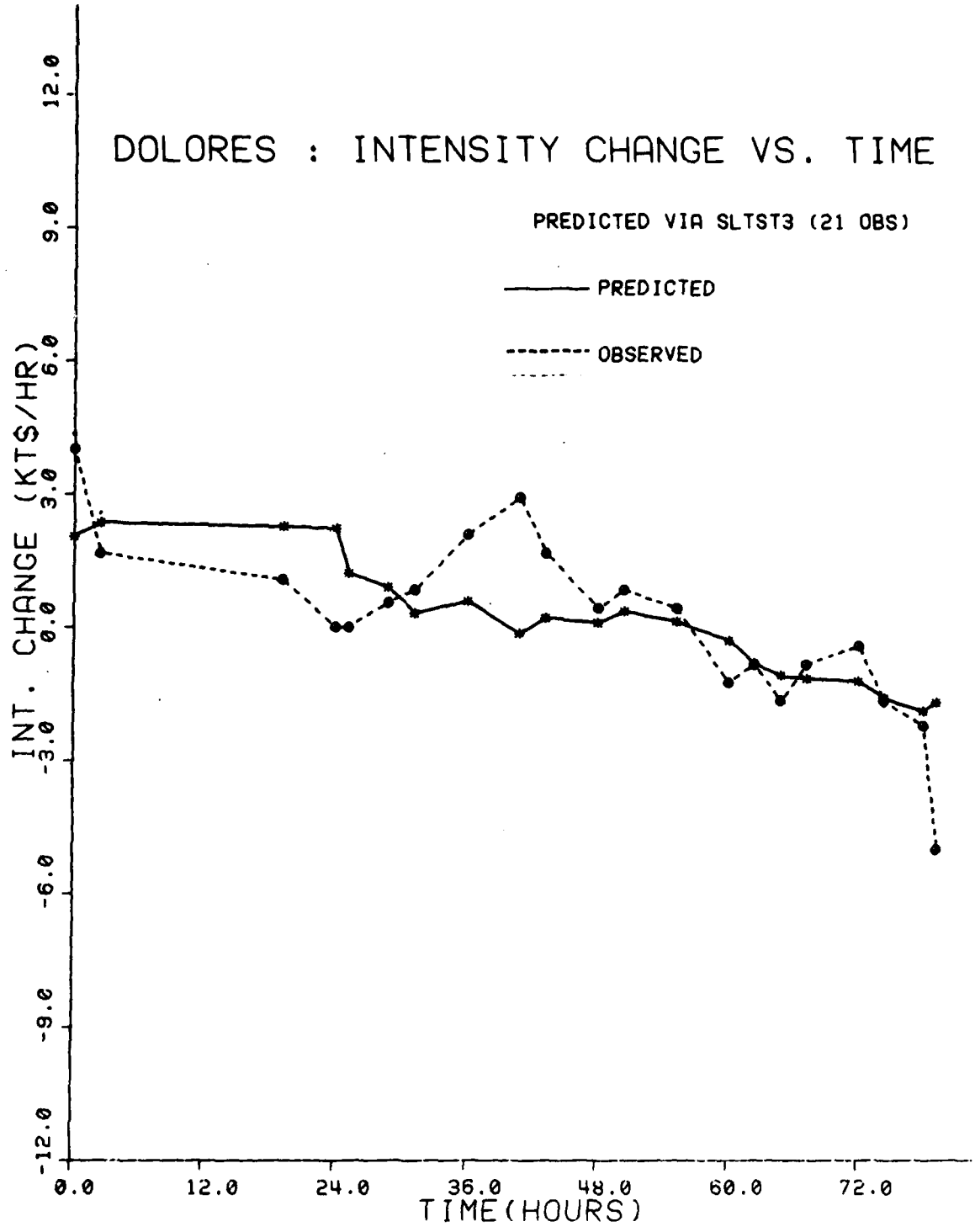

Figure 14. Predicted and observed rates of intensity change for Dolores using three independent variables.

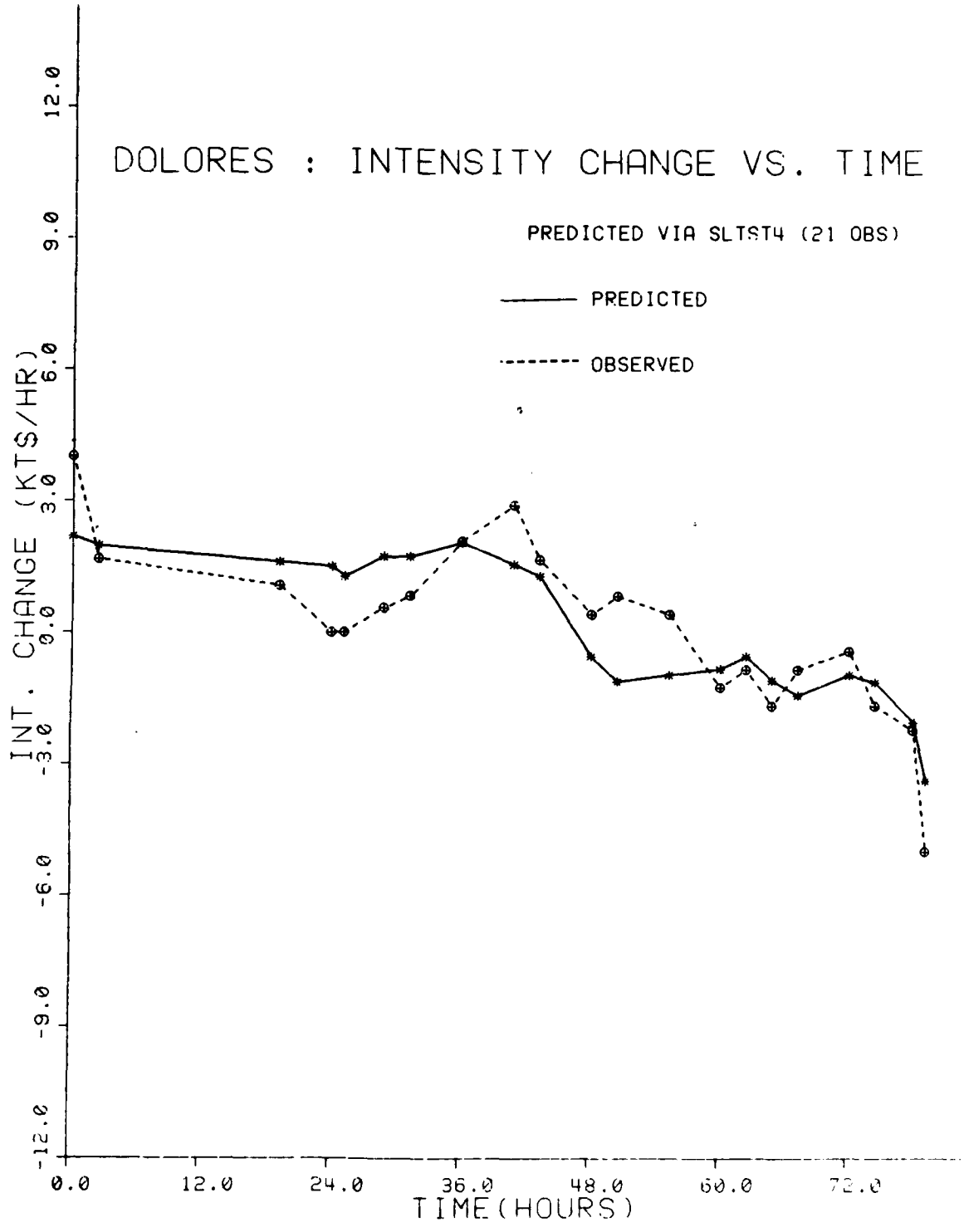

Figure 15. Predicted and observed rates of intensity change for Dolores using four independent variables.

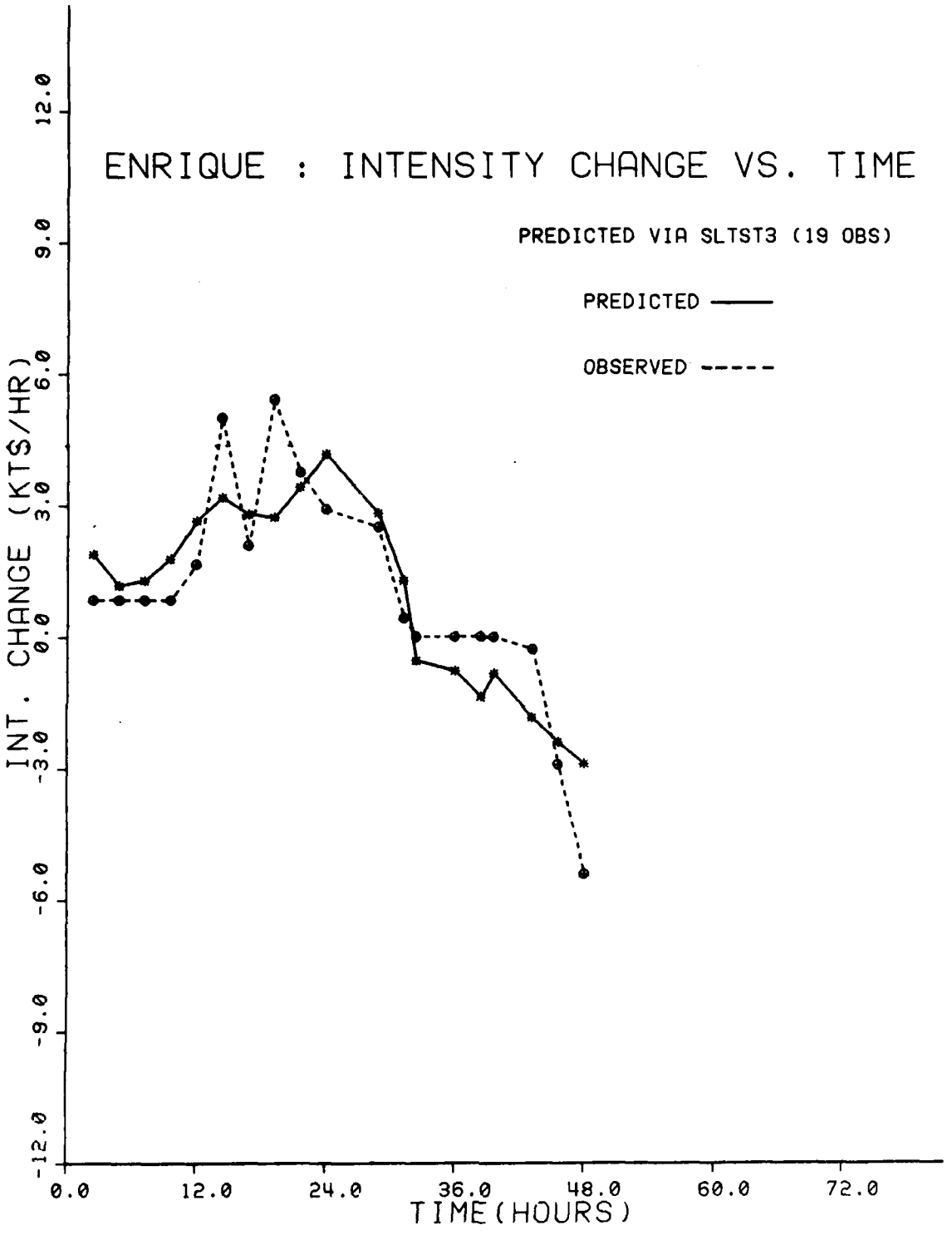

Figure 16. Predicted and observed rates of intensity change for Enrique using three independent variables.

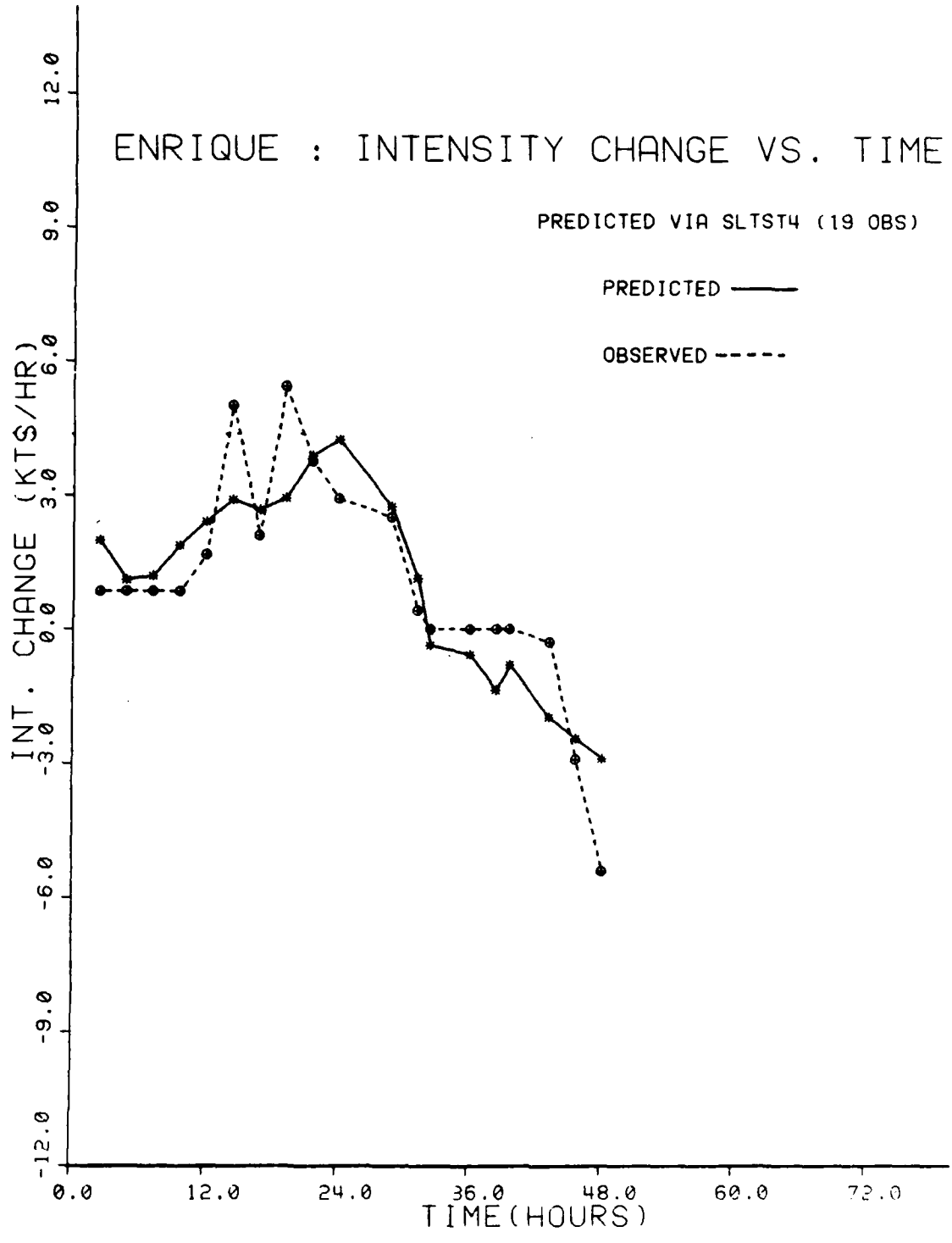

Figure 17. Predicted and observed rates of intensity change for Enrique using four independent variables.

4. BIAS IN RESULTS

The maximum wind speed, and the associated intensity changes derived from them, used as the dependent variables for the regression equations are derived via the Dvorak technique and are only estimates of the maximum wind speeds. The accuracy of the Dvorak technique, based upon independent evaluations (Shewchuk and Weir, 1980), show that the average error of the satellite analysts was approximately 0.5 T-number which translates into an estimated average maximum wind speed error of 5-15 kt, depending on the position on the CI scale. Results from the Joint Typhoon Warning Center (JTWC), based upon post-analysis intensity data, indicate a root-mean-square (RMS) error of 12 kt as documented in the 1st Weather Wing Pamphlet 105-10 (1974).

An error analysis of the SLT predicted maximum wind speeds and intensity changes using the Dvorak estimates as the observed (ground truth) data are shown in Table 7 for Dolores and Table 8 for Enrique.

Table 7. Error analysis for Dolores' four regression cases.

3 INDEPENDENT VARIABLES

OBSVD VMAX	PRED. VMAX	|ERROR|
44.0	44.7	.7
48.0	59.3	11.3
66.0	67.5	1.5
66.0	76.2	10.2
66.0	70.0	4.0
68.0	70.5	2.5
70.0	74.0	4.0
80.0	75.9	4.1
94.0	93.3	.7
98.0	88.5	9.5
100.0	92.6	7.4
102.0	77.6	24.4
104.0	88.9	15.1
98.0	88.6	9.4
96.0	109.1	13.1
92.0	99.9	7.9
90.0	94.8	4.8
88.0	77.7	10.3
84.0	82.5	1.5
76.0	84.3	6.3
70.0	84.3	14.3

Sum of Squared Errors = 1985.0290
Mean Squared Error = 94.5252
Root Mean Squared Error = 9.7224

4 INDEPENDENT VARIABLES

OBSVD VMAX	PRED. VMAX	|ERROR|
44.0	44.5	.5
48.0	59.6	11.6
66.0	68.0	2.0
66.0	76.7	10.7
66.0	70.0	4.0
68.0	69.8	1.8
70.0	72.9	2.9
80.0	74.8	5.2
94.0	92.0	2.0
98.0	87.7	10.3
100.0	93.0	7.0
102.0	78.7	23.3
104.0	89.7	14.3
98.0	89.0	9.0
96.0	108.9	12.9
92.0	99.9	7.9
90.0	95.0	5.0
88.0	77.5	10.5
84.0	82.1	1.9
76.0	84.4	8.4
70.0	85.6	15.6

Sum of Squared Errors = 1975.2220
Mean Squared Error = 94.0582
Root Mean Squared Error = 9.6984

OBSVD RIC	PRED. RIC	|ERROR|
4.0	2.0	2.0
1.7	2.4	.7
1.1	2.3	1.2
.0	2.2	2.2
.0	1.2	1.2
.6	.9	.3
.8	.3	.5
2.1	.6	1.5
2.9	-1.2	3.1
1.7	.2	1.5
.4	.1	.3
.8	.4	.5
.4	.1	.3
-1.3	- .3	1.0
- .8	- .8	.0
-1.7	-1.1	.6
- .8	-1.2	.3
- .4	-1.2	.8
-1.7	-1.6	.1
-2.2	-1.9	.3
-5.0	-1.7	3.3

Sum of Squared Errors = 39.9289
Mean Squared Error = 1.9014
Root Mean Squared Error = 1.3789

OBSVD RIC	PRED. RIC	|ERROR|
4.0	2.2	1.8
1.7	2.0	.3
1.1	1.6	.5
.0	1.5	1.5
.0	1.3	1.3
.6	1.7	1.2
.8	1.7	.9
2.1	2.1	.0
2.9	1.6	1.4
1.7	1.3	.4
.4	- .5	1.0
.8	-1.1	1.9
.4	-1.0	1.4
-1.3	- .8	.4
- .8	- .5	.3
-1.7	-1.1	.6
- .8	-1.4	.6
- .4	-1.0	.5
-1.7	-1.1	.5
-2.2	-2.0	.2
-5.0	-3.4	1.6

Sum of Squared Errors = 22.4912
Mean Squared Error = 1.0710
Root Mean Squared Error = 1.0349

Table 8. Error analysis for Enrique's four regression cases.

3 INDEPENDENT VARIABLES

OBSVD VMAX	PRED. VMAX	|ERROR|
56.0	72.4	16.4
58.0	73.7	15.7
60.0	73.0	13.0
62.0	67.2	5.2
66.0	82.5	16.5
78.0	87.6	9.6
83.0	83.9	.9
96.0	90.9	5.1
105.0	99.3	5.7
112.0	123.3	11.3
124.0	119.3	4.7
125.0	117.6	7.4
125.0	99.6	25.4
125.0	105.5	19.5
125.0	103.2	21.8
125.0	123.7	1.3
124.0	136.2	12.2
117.0	136.1	19.1
104.0	131.0	27.0

Sum of Squared Errors = 4087.2030
Mean Squared Error = 215.1160
Root Mean Squared Error = 14.6668

4 INDEPENDENT VARIABLES

OBSVD VMAX	PRED. VMAX	|ERROR|
56.0	72.5	16.5
50.0	67.7	9.7
60.0	66.4	6.4
62.0	67.4	5.4
66.0	70.0	4.0
78.0	73.7	4.3
83.0	76.0	7.0
96.0	95.0	1.0
105.0	112.7	7.7
112.0	122.4	10.4
124.0	112.9	11.1
125.0	109.6	15.4
125.0	103.3	21.7
125.0	110.2	14.0
125.0	100.6	24.4
125.0	121.7	3.3
124.0	128.4	4.4
117.0	131.5	14.5
104.0	128.1	24.1

Sum of Squared Errors = 3154.8870
Mean Squared Error = 166.0467
Root Mean Squared Error = 12.8859

OBSVD RIC	PRED. RIC	|ERROR|
.8	1.9	1.1
.8	1.2	.3
.8	1.3	.4
.8	1.0	1.0
1.7	2.6	1.0
5.0	3.2	1.8
2.1	2.8	.7
5.4	2.7	2.7
3.8	3.4	.3
2.9	4.2	1.3
2.5	2.8	.3
.4	1.3	.9
.0	- .5	.5
.0	- .8	.8
.0	-1.4	1.4
.0	- .8	.8
- .3	-1.8	1.6
-2.9	-2.4	.5
-5.4	-2.9	2.5

Sum of Squared Errors = 29.3720
Mean Squared Error = 1.5459
Root Mean Squared Error = 1.2434

OBSVD RIC	PRED. RIC	|ERROR|
.8	2.0	1.1
.8	1.1	.3
.8	1.2	.4
.8	1.9	1.0
1.7	2.4	.7
5.0	2.9	2.1
2.1	2.7	.6
5.4	2.9	2.5
3.8	3.9	.1
2.9	4.2	1.3
2.5	2.7	.2
.4	1.1	.7
.0	- .4	.4
.0	- .6	.6
.0	-1.4	1.4
.0	- .8	.8
- .3	-2.0	1.7
-2.9	-2.4	.5
-5.4	-2.9	2.5

Sum of Squared Errors = 28.8347
Mean Squared Error = 1.5176
Root Mean Squared Error = 1.2319

5. CONCLUSIONS AND RECOMMENDATIONS

The foregoing predictive equations are not meant to be used as prognostic equations, rather they are a measure of the feasibility of the SLT's usefulness as a forecast tool. The significant differences for the two storm's set of regression coefficients leads to the question as to which set of coefficients to use for a given storm. Gentry et al. (1978) found it necessary to stratify the storms based upon their current intensity estimate, with an equation for weak storms ($V_{max} \leq 65$ kt) and one for more intense storms. The stratification of the storms is useful only for intensity forecasts. More work needs to be done with independent data sets before any statistically significant results may be ascertained.

In the case of maximum wind speed estimation, the storm to storm variability in the amount and structure of the convective activity appears to be too large for the development of an objective technique utilizing SLT-derived parameters to accomplish such a task. This result agrees with that of Brody and Tsui (1982) in their attempt to predict maximum wind speeds using the technique described by Gentry et al. (1978).

The outlook for the development of an objective technique for predicting intensity changes, however, appears promising. SLT-derived parameters used in conjunction with parameters derived from the tropical cyclone intensity forecast program (Brody and Tsui) using the algorithm developed by Gentry et al. may provide the answer. Other parameters such as latitude of the storm, time of year, and oceanic basin may help in explaining more of the observed variance. Inclusion of the current intensity estimate into the forecast scheme may result in a more accurate intensity change estimate, although with somewhat less objectivity.

Smith (1972) used low and high level cloud motions derived from ATS-11 satellite images to construct fields of radial and tangential wind components, areal relative vorticity, and areal divergence for various times during the life cycle of Hurricane Celia (1970). Using his values for the low cloud level and the relations described by Lahiri, (i.e., $\nabla \cdot V/ = -a$ and $V_r/V_o = -a$) the computed ranged for the spiral constants for Hurricane Celia were found to be $0.2 < a < 0.5$ for large radii. This translates to inflow angles, α, ranging from $11.3^o < \alpha < 26.6^o$ for the wind field spirals. Comparing this with the range of SLT-derived cloud band spiral constants and inflow angles of $0.3 < a < 0.8$ and $16.7^o < \alpha < 38.7^o$ respectively, it appears that the spirals traced out by the cloud bands have a much larger inflow angle than that of the wind field. The assumption made by Lahiri, that the cloud band spirals can be used as a tracer of the wind field spirals appears to be invalid.

The current SLT has only limited effectiveness in isolating spiral banding features from the large and sometimes amorphous cloud masses associated with tropical cyclones. The current method isolates a spiral band by enhancing the satellite image. The spiral band must be clearly distinguishable from cloud features not associated with the spiral band. The resulting transformed spiral band must then be readily subsetted (excluded) from the cloud masses not associated with the spiral band so that the least squares line will be applied to the band only. This process, at times, cannot isolate obvious spiral features necessary to derive the SLT parameters.

A new SLT is being developed which will allow the user to define a spiral feature using the graph pen and pad. This eliminates the necessity to clearly isolate the spiral band, as with the current SLT, and does not require the image to be transformed, pixel by pixel, into spiral coordinates, but rather a spiral equation can be fitted to the curve traced out with the graph pen. This allows for the same statistical parameters to be calculated as well as the objective determination of the spiral constant, center, and offset radii. More important, however, is

that the new method allows for the use of the FFT's, at specified points both along and normal to the spiral band, to determine information concerning cloud size and spacing previously unavailable due to distortions caused by the current SLT transformation algorithm.

The results of this project are sufficiently promising to warrant further investigation into the development of an objective technique to determine intensity changes employing parameters derived from the new SLT and those derived from the tropical cyclone intensity forecast algorithm.

REFERENCES

Brody, R., and T. Tsui, 1982: Personal communication.

Dvorak, V., 1975: Tropical cyclone intensity analysis and forecasting from satellite imagery. Mon. Wea. Rev, 103, 420-430.

Gentry, C., E. Rodgers, J. Steranka, W. Schenk, 1978: Predicting tropical cyclone intensity using satellite measured equivalent blackbody temperatures of cloud tops. NASA Tech. Mem. 79645, 37 pp.

Gonzalez, R. C., and P. Wintz, 1977: Digital image processing. Addison-Wesley Publishing Co., Inc., Massachusetts, 431 pp.

Gunther, E., 1980: Eastern North Pacific tropical cyclones of 1979. Mon. Wea. Rev., 108, 631-641.

Hughes, L., 1952: On the low-level wind structure of tropical storms. Journ. Meteor., 9, 422-428.

Lahiri, A., 1981: A study of cloud spirals of tropical cyclones. MAUSAM, 32, 155-158.

Milne-Thompson, L., 1960: Theoretical hydrodynamics. MacMillan Company, New York, 660 pp.

Peterson, V., W. Hubert, and R. Langland, 1982: Adaptation of the tropical cyclone spiral linearization techniques to extratropical regions. Ocean Data Systems, Inc., Rept. No. N66856-81MD-00022, 58 pp.

Schramm, W., P. Zeleny, R. Nagle, and A. Weinstein, 1982: The Navy SPADS, a second generation environmental display system. Ninth Conference Weather Forecasting and Analysis, Seattle, WA.

Senn, H., and H. Hiser, 1957: Tracking hurricanes with radar. Proc. Sixth Weather Radar Conf., Boston, Amer. Met. Soc., 165-170.

Shewchuk, J., and R. Weir, 1980: An evaluation of the Dvorak technique for estimating tropical cyclone intensities from satellite imagery. NOCC/JTWC Tech. Note 80-2, 25 pp.

Smith, C., 1972: On the intensification of Hurricane Celia (1970). NOAA Tech. Mem. ERL NHRL-100, 35 pp.

DISTRIBUTION LIST

OFFICE OF NAVAL RESEARCH
CODE 422AT
ARLINGTON, VA 22217

OFFICE OF NAVAL RESEARCH
CODE 420
ARLINGTON, VA 22217

OFFICE OF NAVAL RESEARCH
COASTAL SCIENCES PROGRAM
CODE 422CS
ARLINGTON, VA 22217

CHIEF OF NAVAL OPERATIONS
(OP-952)
U.S. NAVAL OBSERVATORY
WASHINGTON, DC 20390

CHIEF OF NAVAL OPERATIONS
NAVY DEPT. OP-986G
WASHINGTON, DC 20350

CHIEF OF NAVAL MATERIAL
NAVY DEPT. MAT-0724
WASHINGTON, DC 22332

NAVAL DEPUTY TO THE
ADMINISTRATOR, NOAA
RM. 200, PAGE BLDG. #1
3300 WHITEHAVEN ST. NW
WASHINGTON, DC 20235

COMNAVOCEANCOM
NSTL STATION
BAY ST. LOUIS, MS 39529

COMMANDING OFFICER
NAVWESTOCEANCEN
BOX 113
PEARL HARBOR, HI 96860

COMMANDING OFFICER
U.S. NAVOCEANCOMCEN
BOX 12, COMNAVMARIANAS
FPO SAN FRANCISCO 96630

COMMANDER (2)
NAVAIRSYSCOM
ATTN: LIBRARY, AIR-00D4
WASHINGTON, DC 20361

COMMANDER
NAVAIRSYSCOM (AIR-333)
WASHINGTON, DC 20361

COMMANDER
NAVAIRSYSCOM
MET. SYS. DIV. (AIR-553)
WASHINGTON, DC 20360

USAFETAC/TS
SCOTT AFB, IL 62225

AFGL/LY
HANSCOM AFB, MA 01731

DIRECTOR (12)
DEFENSE TECH. INFORMATION
CENTER, CAMERON STATION
ALEXANDRIA, VA 22314

DIRECTOR
NATIONAL HURRICANE CENTER
NOAA, GABLES ONE TOWER
1320 S. DIXIE HWY
CORAL GABLES, FL 33146

CHIEF, SCIENTIFIC SERVICES
NWS, PACIFIC REGION
P.O. BOX 50027
HONOLULU, HI 96850

METEOROLOGIST IN CHARGE
WEATHER SERVICE FORECAST
OFFICE, NOAA
660 PRICE AVE.
REDWOOD CITY, CA 94063

DIRECTOR, CENTRAL PACIFIC
HURRICANE CENTER
NWS, NOAA

METEOROLOGIST IN CHARGE
WEATHER SERVICE FORECAST
OFFICE, NOAA
HONOLULU INTL. AIRPORT
HONOLULU, HI 96819

CHIEF
MESOSCALE APPLICATIONS
BRANCH, NESS
1225 W. DAYTON
MADISON, WI 53562

DIRECTOR, NATIONAL HURRICAN
RESEARCH LAB (AOML)
1320 S. DIXIE HWY.
CORAL GABLES, FL 33146

DIRECTOR
TECHNIQUES DEVELOPMENT LAB
GRAMAX BLDG.
8060 13TH ST.
SILVER SPRING, MD 20910

LABORATORY FOR ATMOSPHERIC
SCIENCES, NASA
GODDARD SPACE FLIGHT CENTER
GREENBELT, MD 20771

CHAIRMAN, METEOROLOGY DEPT.
CALIFORNIA STATE UNIVERSITY
SAN JOSE, CA 95192

COLORADO STATE UNIVERSITY
ATMOSPHERIC SCIENCES DEPT.
ATTN: DR. ROGER PIELKE
FT COLLINS, CO 80523

DIRECTOR, REMOTE SENSING LA
UNIVERSITY OF MIAMI
P.O. BOX 248003
CORAL GABLES, FL 33124

FLORIDA STATE UNIVERSITY
ENVIRONMENTAL SCIENCES DEPT
TALLAHASSEE, FL 32306

UNIVERSITY OF HAWAII
METEOROLOGY DEPT.
2525 CORREA ROAD
HONOLULU, HI 96822

UNIVERSITY OF MARYLAND
METEOROLOGY DEPT.
COLLEGE PARK, MD 20742

CHAIRMAN
METEOROLOGY DEPT.
UNIVERSITY OF UTAH
SALT LAKE CITY, UT 84112

UNIVERSITY OF WASHINGTON
ATMOSPHERIC SCIENCES DEPT.
SEATTLE, WA 98195

CHAIRMAN, METEOROLOGY DEPT.
UNIVERSITY OF WISCONSIN
METEORO. & SPACE SCI. BLDG.
1225 W. DAYTON ST.
MADISON, WI 53706

COLORADO STATE UNIVERSITY
ATMOSPHERIC SCIENCES DEPT.
ATTN: LIBRARIAN
FT. COLLINS, CO 80521

COLORADO STATE UNIVERSITY
ATMOSPHERIC SCIENCES DEPT.
ATTN: DR. WILLIAM GRAY
FT. COLLINS, CO 80523

DIRECTOR, JTWC
BOX 17
FPO SAN FRANCISCO 96630

BUREAU OF METEOROLOGY
ATTN: LIBRARY
BOX 1289K, GPO
MELBOURNE, VIC, 3001
AUSTRALIA

SCHOOL OF PHYS. & GEOSCIENCES
WESTERN AUSTRALIAN INSTITUTE
OF TECHNOLOGY
HAYMAN ROAD
SOUTH BENTLEY 6102, AUSTRALIA


4-
DT